UCLA
COMPUTATIONAL AND APPLIED MATHEMATICS

Numerical Simulation of Inviscid Detonation Waves With Finite Rate Chemistry

Vinh T. Ton
Ann R. Karagozian
Bjorn E. Engquist
Stanley J. Osher

October 1991

CAM Report 91-22

Department of Mathematics
University of California, Los Angeles
Los Angeles, CA. 90024-1555

NUMERICAL SIMULATION OF INVISCID DETONATION WAVES WITH FINITE RATE CHEMISTRY

Vinh T. Ton and Ann R. Karagozian
Department of Mechanical, Aerospace, and Nuclear Engineering

Bjorn E. Engquist and Stanley J. Osher [1]
Department of Mathematics

University of California, Los Angeles
Los Angeles, CA 90024-1597

Abstract

A new, efficient, and accurate numerical method for solving hyperbolic conservation laws with stiff source terms is developed to simulate inviscid, chemically reacting flows. In the first part of the method, an essentially non-oscillatory (ENO) shock capturing scheme using numerical fluxes and TVD/Runge-Kutta time discretization is applied to solve the conservation equations without the inclusion of source terms. The reaction chemistry in the absence of fluid motion is then solved in the second step. A new technique for proper treatment of the stiff source terms is included in the second step in order to avoid stiffness problems, so that correct solution of stiff combustion waves can be obtained, even for large time steps and grid sizes. Numerical results for one-dimensional shock tube and ZND detonation waves for alternative test cases are obtained, with excellent correspondence between numerical predictions and analytical and experimental data.

[1]Research supported by: DARPA grant in the ACMP Program; and ARO# DAAL03-91-00162.

1. Introduction

Modeling of non-equilibrium gas-dynamics is frequently hampered by numerical difficulties arising from the stiffness of the chemical source terms. Stiffness problems can lead to solutions yielding non-physical waves with incorrect wave speeds and strengths. These non-physical phenomena have been observed numerically by Colella, Majda and Roytburd [1]; Ben-Artzi [2]; and LeVeque and Yee [3]. For flows containing contact surfaces separating species with different ratios of specific heats, numerical experiments show that erroneous oscillations and computational inaccuracies occur around contact discontinuities (see Abgrall [4], Chargy et al. [5], and Karni [6]).

In this paper a new, efficient and accurate numerical method for solving hyperbolic conservation laws with or without stiff source terms is developed to simulate inviscid and chemically reacting or mixing flows. A new technique for proper treatment of the source terms, developed by Engquist and Sjogreen [7], is included in this method in order to avoid the aforementioned stiffness problem. With this method, correct solution of stiff combustion waves can be obtained, even for large time steps and grid sizes. The numerical difficulty at a contact discontinuity for mixing flows will also be addressed, and we will show how to eliminate this problem.

The accuracy of the method will be demonstrated by three test cases. The first test case is the simulation of the Sod's shock tube problem with a diaphragm separating two non-reactive ideal gases with different ratios of specific heats. The second test case is the simulation of a Chapman-Jouguet detonation wave with one-step kinetics. Finally, the ignition processes in hydrogen-oxygen-argon mixtures behind a shock wave reflected from a rigid wall are simulated in the third test case. A detailed 37-step chemical reaction relating 8 species is used in this simulation.

2. Governing Equations

The governing equations for one-dimensional, multi-component flow of inviscid, compressible, and reactive gaseous species are the Euler equations for the gas mixture and mass conservation equations for each species. The Euler equations are the conservation laws for mass, momentum, and energy. For a mixture of NS species, the governing equations in vector form can be written as

$$\mathbf{U}_t + \mathbf{F}_x = \mathbf{S} \tag{2.1}$$

where **U**, **F**, and **S** are vectors given by

$$\mathbf{U} = \begin{pmatrix} \rho \\ \rho u \\ e \\ \rho Y_1 \\ \rho Y_2 \\ \vdots \\ \rho Y_{NS-1} \end{pmatrix} \quad \mathbf{F} = \begin{pmatrix} \rho u \\ \rho u^2+p \\ (e+p)u \\ \rho u Y_1 \\ \rho u Y_2 \\ \vdots \\ \rho u Y_{NS-1} \end{pmatrix} \quad \mathbf{S} = \begin{pmatrix} 0 \\ 0 \\ 0 \\ \dot{\omega}_1 \\ \dot{\omega}_2 \\ \vdots \\ \dot{\omega}_{NS-1} \end{pmatrix} \tag{2.2}$$

Components of vector **U** are called conservative variables, and **F** contains the conserved fluxes. Here, ρ is the mixture density, u is the mixture velocity, e is the total energy per unit volume, p is the mixture total pressure, Y_i is the mass fraction of species i, and $\dot{\omega}_i$ is the mass production rate of species i.

We will assume that all species satisfy the ideal gas equation. The equation of state is

$$p = \rho R_u T \sum_{i=1}^{NS} \frac{Y_i}{W_i} \tag{2.3}$$

where R_u is the universal gas constant, T is the mixture temperature, and W_i is molecular weight of species i.

The total energy per unit volume can be expressed as

$$e = \frac{p}{(\gamma-1)} + \frac{1}{2}\rho u^2 + \sum_{i=1}^{NS} \rho Y_i h_{f,i}^0 \tag{2.4}$$

where $h^0_{f,i}$ is the heat of formation of species i. γ is the ratio of specific heats of the mixture; γ will be defined in the next section.

The total enthalpy for the mixture is

$$H = \frac{e + p}{\rho} \tag{2.5}$$

3. Thermodynamic Properties of the Mixture

The specific heat at constant pressure for species i, $c_{p,i}$, is taken to be in the form of a polynomial fit in temperature,

$$c_{p,i} = \frac{R_u}{W_i} \sum_{n=1}^{N} a_{n,i} T^{(n-1)} \tag{3.1}$$

The ratio of specific heats of species i is then

$$\gamma_i = \frac{c_{p,i}}{c_{p,i} - \frac{R_u}{W_i}} \tag{3.2}$$

The mass weighted mean specific heat at constant pressure of the mixture is defined as

$$\overline{c_p} = \sum_{i=1}^{NS} c_{p,i} Y_i \tag{3.3}$$

and the mean molecular weight of the mixture is defined as

$$\overline{W} = \frac{1}{\sum_{i=1}^{NS} \frac{Y_i}{W_i}} \tag{3.4}$$

We define the ratio of specific heats of the mixture in the same way as for an individual species (γ_i), but using the mass weighted mean specific heat and mean molecular weight of he mixture :

$$\gamma = \frac{\overline{c_p}}{\overline{c_p} - \frac{R_u}{\overline{W}}} \tag{3.5}$$

Thus, in terms of conservative variables, γ can be expressed as

$$\gamma = 1 + \frac{\frac{\rho}{W_{NS}} + \sum_{i=1}^{NS-1} \Delta(\frac{1}{W_i})\rho Y_i}{\frac{c_{p,NS}\rho}{R_u} - \frac{\rho}{W_{NS}} + \sum_{i=1}^{NS-1} (\Delta(\frac{c_{p,i}}{R_u}) - \Delta(\frac{1}{W_i}))\rho Y_i} \tag{3.6}$$

where

$$\Delta(\frac{1}{W_i}) = \frac{1}{W_i} - \frac{1}{W_{NS}} \tag{3.7}$$

$$\Delta(\frac{c_{p,i}}{R_u}) = \frac{c_{p,i}}{R_u} - \frac{c_{p,NS}}{R_u} \tag{3.8}$$

Note that, in terms of conservative variables, γ is a function of ρ, ρY_1, ρY_2, ... , ρY_{NS-1} . Derivatives of γ with respect to the conservative variables are given below

$$\frac{\partial \gamma}{\partial \rho} = \frac{\sum_{i=1}^{NS-1} (\frac{c_{p,i}}{W_{NS}R_u} - \frac{c_{p,NS}}{R_u W_i})\rho Y_i}{\left\{\frac{c_{p,NS}\rho}{R_u} - \frac{\rho}{W_{NS}} + \sum_{i=1}^{NS-1} (\Delta(\frac{c_{p,i}}{R_u}) - \Delta(\frac{1}{W_i}))\rho Y_i\right\}^2} \tag{3.9}$$

$$\frac{\partial \gamma}{\partial(\rho Y_i)} = \frac{\rho\frac{c_{p,NS}}{R_u}\Delta(\frac{1}{W_i}) - \frac{\rho}{W_{NS}}\Delta(\frac{c_{p,i}}{R_u}) + \Delta(\frac{1}{W_i})\sum_{j=1,j\neq i}^{NS-1} \Delta(\frac{c_{p,j}}{R_u})\rho Y_j - \Delta(\frac{c_{p,i}}{R_u})\sum_{j=1,j\neq i}^{NS-1} \Delta(\frac{1}{W_j})\rho Y_j}{\left\{\frac{c_{p,NS}\rho}{R_u} - \frac{\rho}{W_{NS}} + \sum_{i=1}^{NS-1} (\Delta(\frac{c_{p,i}}{R_u}) - \Delta(\frac{1}{W_i}))\rho Y_i\right\}^2} \tag{3.10}$$

It is interesting to note that

$$\frac{\partial \gamma}{\partial \rho} = -\sum_{i=1}^{NS-1} Y_i \frac{\partial \gamma}{\partial(\rho Y_i)} \tag{3.11}$$

4. Numerical Method

Most researchers employ a fractional step algorithm to solve the system of hyperbolic conservation laws with stiff source terms (e.g., [1,8]). In this section, we will extend this algorithm to solve the system of equations (2.1) in order to eliminate the aforementioned stiffness problems.

The fractional step algorithm involves the following steps :

i) First step :

In this step, we allow the species to convect passively, i.e., we solve the homogeneous system of equations (2.1) :

$$\mathbf{U}_t + \mathbf{F}_x = 0 \tag{4.1}$$

The work of Shu and Osher [9], using the essentially non-oscillatory (ENO) shock capturing scheme based on numerical fluxes and TVD/Runge-Kutta time discretization, is extended to solve the multi-component flow of (4.1).

ii) Second step :

The stiff ordinary differential equations describing the chemical kinetics are solved in this step.

We have

$$\frac{\partial \rho}{\partial t} = 0 \tag{4.2a}$$

$$\frac{\partial(\rho Y_i)}{\partial t} = \dot{\omega}_i \qquad i=1,...,NS-1 \tag{4.2b}$$

Combining the above equations, we obtain

$$(Y_i)_t = \frac{\dot{\omega}_i}{\rho} \qquad i=1,...,NS-1 \tag{4.3}$$

iii) Third step :

The above steps are coupled together by updating the primitive variables using the new values of Y_i obtained from the second step.

There are remaining stiffness problems, however, due to the interaction between the variables in the above steps. For a very fine mesh and time step, a stiff combustion wave can be resolved; however, for realistic choices of time step and grid size, non-physical waves with incorrect wave speed and strength will be obtained (see [1-3]). This numerical phenomenon is due to the non-equilibrium points at the shock front introduced by conservative shock capturing schemes as shown by [3]. Even with modern shock capturing schemes which are able to resolve the shock front with only one or two cells, the corresponding temperature of these points can prematurely ignite the chemical reaction.

Since, for a detonation wave, no chemical reaction should start before the shock wave has passed through, we want to prevent these non-equilibrium points from triggering the reaction. Engquist and Sjogreen [7] propose a simple solution to this problem by modifying the temperature at grid point i as

$$T_i = \min (T_{i+d}, T_{i-d}) \tag{4.4}$$

where d approximately equals the number of non-equilibrium points. We modify the second step of the above algorithm by applying equation (4.4) when calculating the right-hand-side of the system of equations (4.3).

Higher order accuracy can be obtained by extrapolating T_i from its neighboring cells. Filters to identify the non-equilibrium points can also be used. We will not explore these techniques further since (4.4) already works well for the present applications.

5. Numerical results

5.1) Multi-Component Mixing Flow

The first test problem that we study is Sod's shock tube problem. The shock tube is open at both ends with a diaphragm separating two non-reactive ideal gases with different ratios of specific heats. The initial data (non-dimensionalized) are

$\rho_l = 1$	$\rho_r = 0.125$
$p_l = 1$	$p_r = 0.1$
$u_l = 0$	$u_r = 0$
$\gamma_l = 1.4$	$\gamma_r = 1.2$
$Y_{1,l} = 1$	$Y_{1,r} = 0$
$Y_{2,l} = 0$	$Y_{2,r} = 1$

This same test problem has been studied in [4-6]. These researchers used a different model for the ratio of specific heats of the mixture (see [10]). They also assumed that the specific heats at constant volume for gases on the left and on the right of the diaphragm were the same. Figure 1 presents the results by Larrouturou [11] which employ Roe's scheme with first order accuracy. Figure 2 presents the results by Karni [6] which incorporates a second order upwind scheme. From these results, we can see that these methods have difficulties resolving the contact discontinuity; there is a non-physical step in the velocity profile and an erroneous dip in the density profile across the contact discontinuity.

For the present calculation, we use γ as described in section 3. We allow air to represent the ideal gas on the left of the diaphragm. The dimensional specific heat at constant pressure and molecular weight for air (species 1) are, respectively,

$$c_{p,1} = 1.007 \times 10^7 \text{ erg/gK}$$

$$W_1 = 28.97 \text{ g/mol}$$

The region to the right of the diaphragm contains an ideal gas with γ=1.2. Assuming that the initial temperatures have equilibrated across the diaphragm (T_l=T_r), we can calculate the gas properties for species 2 as

$$c_{p,2} = 2.152 \times 10^7 \ \text{erg/gK}$$

$$W_2 = 23.176 \ \text{g/mol}$$

In this calculation, we use 100 cells with a uniform spacing of Δx=0.01. The results are presented in Figure 3. In this figure, the open circles represent the numerical solutions with third order accuracy as obtained by the present method; the solid lines are exact analytical solutions to the problem.

Excellent agreement between numerical results and analytical solutions is achieved. The aforementioned numerical difficulties do not appear in this solution. We suggest that the numerical difficulties as obtained in [4-6] may be due to

i) a different model for γ and its derivatives, or

ii) the assumption that $c_{v,1} = c_{v,2}$, or

iii) a combination of i) and ii).

5.2) Chapman-Jouguet Detonation Wave with One-Step Kinetics

A stiff Chapman-Jouguet (C-J) detonation wave is simulated in this section. As a test case, we simulate ozone decomposition. Following [1-2 and 12], we assume that the unburned (species 1) and burned (species 2) gases are perfect gases with constant ratios of specific heats; γ=1.4 is used for both species. A single one-step kinetic mechanism is assumed; we use a simplified Arrhenius model where the reaction rate is a step function depending on temperature. The mass production rate as expressed in (2.2) thus becomes

$$\dot{\omega}_1 = -k\rho \qquad (5.1)$$

with

$$k = KY_1H(T-T_c) \tag{5.2}$$

where T_c is the critical temperature and

$$H(x)= \begin{cases} 1 & x>0 \\ 0 & x\leq 0 \end{cases} \tag{5.3}$$

Hence, the ODE (4.3) can be integrated exactly, and the mass fraction of unburned gas can be calculated by

$$Y_1^{n+1} = Y_1^n \exp[-K\Delta tH] \tag{5.4}$$

The constants are given as

$$T_c = 500 \text{ K}$$

$$K = 5.825 \times 10^9 \text{ sec}^{-1}$$

$$h_{f,1}^0 = 5.196 \times 10^9 \text{ dynes-cm/g}$$

The initial states for unburned gas are

$$\rho_0 = 1.201 \times 10^{-3} \text{ g/cm}^3$$

$$p_0 = 8.321 \times 10^5 \text{ dynes/cm}^2$$

$$u_0 = 0$$

$$Y_1 = 1$$

$$Y_2 = 0$$

The computed C-J initial states for the burned gas are

$$\rho_{CJ} = 1.945 \times 10^{-3} \text{ g/cm}^3$$

$$p_{CJ} = 6.270 \times 10^6 \text{ dynes/cm}^2$$

$$u_{CJ} = 4.162 \times 10^4 \text{ cm/sec}$$

$$Y_1 = 0$$

$$Y_2 = 1$$

Finally, the speed of the C-J detonation wave is 1.088×10^5 cm/sec.

We use 100 cells of uniform spacing. To follow the moving wave and to keep the reaction zone roughly at the middle of the mesh, we keep eliminating cells at the left and creating new cells at the right.

For a very fine mesh and step size of

$$\Delta x = 5 \times 10^{-6} \text{ cm}$$

$$\Delta t = 5 \times 10^{-12} \text{ s}$$

the ZND detonation wave with a von Neumann spike is resolved correctly without using the technique in [7] as discussed in section 4. The results at 1×10^{-8} seconds are presented in Figure 4. With the inclusion of equation (4.4), the solution only changes slightly.

Now, for a realistic choice of time step and grid size of

$$\Delta x = 5 \times 10^{-4} \text{ cm}$$

$$\Delta t = 1 \times 10^{-10} \text{ s}$$

the results at 1×10^{-6} seconds are shown in Figure 5. In this figure, the open circles represent the correct solution of the detonation wave as obtained by the present method. If the source term is not treated properly (as done, for example, in [1-2]), non-physical solutions are obtained; these are shown by the asterisk symbols in Figure 5.

5.3) Detonation Wave with Multi-Step Kinetics

The ignition processes in hydrogen-oxygen-argon mixtures behind a shock wave reflected from a rigid wall are simulated in this section. This simulation is based on the reflected shock tube experiments performed by Cohen and Larsen [13]. The corresponding numerical simulation is computed by Oran et al. [8], who use the flux-corrected transport method along with an adaptive grid in their solutions.

We use a detailed 37-step chemical reaction relating 8 species (H_2, O_2, O, H, OH, HO_2, H_2O_2 and H_2O), described by Maas and Warnatz [14], in the present simulation. The general set of chemical reactions k can be written as

$$\sum_{i=1}^{N} \nu'_{ik} M_i \leftrightarrow \sum_{i=1}^{N} \nu''_{ik} M_i \tag{5.5}$$

where M_i is the chemical symbol for species i, ν'_{ik} and ν''_{ik} are the stoichiometric coefficients for species i appearing as reactant and product, respectively, N is the total number of species involved, and k_{fk} and k_{bk} are the forward and backward reaction rate constants, respectively. The mass production rate of species i from the reaction step k is

$$\dot{\omega}_{ik} = W_i(\nu''_{ik}-\nu'_{ik})[k_{fk}\prod_{j=1}^{N} c_j^{\nu'_{jk}} - k_{bk}\prod_{j=1}^{N} c_j^{\nu''_{jk}}] \tag{5.6}$$

where c_i is the molar concentration of species i.

The system of ordinary differential equations (4.3) describing the chemical kinetics is solved using the CHEMKIN scheme developed by Kee et al. [15]. Heats of formation have been taken from the JANAF tables [16].

The left-hand boundary of the shock tube is a rigid wall, and zero-derivative of primitive variables is applied at the right-hand boundary. The initial mixture of the gases is

$$H_2 : O_2 : Ar \ / 2 : 1 : 7 /$$

The initial condition is an incident shock, at x = 3 cm, traveling to the left. The states behind the incident shock are

$$\rho_2 = 2.0539 \times 10^{-4} \text{ g/cm}^3$$

$$p_2 = 3.6680 \times 10^{5} \text{ dynes/cm}^2$$

$$u_2 = -5.1564 \times 10^{4} \text{ cm/sec}$$

The initial states for the undisturbed region are

$$\rho_1 = 7.20486 \times 10^{-5} \text{ g/cm}^3$$

$$p_1 = 7.17277 \times 10^4 \text{ dynes/cm}^2$$

$$u_1 = 0$$

We note that the above initial states are only slightly different from those in [8].

We use a coarse grid of 100 cells with uniform spacing ($\Delta x = 0.12$ cm). Since the combustion wave in this problem is not stiff, equation (4.4) is not needed. Figure 6 presents the calculated positions of the incident shock front, the reflected shock front, the reaction wave, the transmitted detonation wave, and the contact discontinuity as a function of time. The incident shock is reflected at the rigid wall at about 35 μs. The reaction wave accelerates to a detonation at about 140 μs, then it merges with the reflected shock front at 180 μs. The transmitted detonation wave and contact discontinuity are decelerated due to the incoming flow. Figure 7 presents the density profiles at 115, 144, 166 and 211 μs. Figure 8 presents the density, pressure, velocity and temperature profiles at 166 μs. Mass fraction profiles of H_2, O_2, OH, H_2O at 166 μs are shown in Figure 9.

In general, the present results are in very good agreement with those measured from the experiment by [13] and numerically calculated in [8], as shown in Figures 10 a and 10 b.

The attractiveness of the present methodology is that severe limitations on spatial and temporal step sizes are eliminated, thus providing a computationally less-expensive means of carrying out detonation calculations. Ongoing and future work on the development of these efficient numerical schemes focuses on simulation of two-dimensional, compressible reacting flowfields.

References

1. Colella, P., Majda, A., and Roytburd, V., "Theoretical and Numerical Structure for Reacting Shock Waves," SIAM J. Sci. Stat. Comput., 7, 1059-1080, October 1986.

2. Ben-Artzi, M., "The Generalized Riemann Problem for Reactive Flows," J. Comput. Phys., 81, 70-101, 1989.

3. LeVeque, R. J. and Yee, H. C., "A Study of Numerical Methods for Hyperbolic Conservation Laws with Stiff Source Terms," J. Comput. Phys., 86, 187-210, 1990.

4. Abgrall, R., Recherche Aerospatiale, 6, 31, 1988.

5. Chargy, D., Abgrall, R., Fezoui, L., and Larrouturou, B., "Comparisons of Several Numerical Schemes for Multi-component One-dimensional Flows," INRIA Report 1253, 1990.

6. Karni, S., "Multi-component Flow Calculations by a Consistent Primitive Algorithm," submitted for publication, 1991.

7. Engquist, B. and Sjogreen, B., "Robust Difference Approximations of Stiff Inviscid Detonation Waves," UCLA CAM Report 91-03, March 1991.

8. Oran, E. S., Young, T. R., Boris, J. P., and Cohen, A., "Weak and Strong Ignition. I. Numerical Simulations of Shock Tube Experiments," Comb. and Flame, 48, 135-148, 1982.

9. Shu, C. W. and Osher, S. J., " Efficient Implementation of Essentially Non-oscillatory Shock-Capturing Schemes, II," J. Comput. Phys., 83, 32-78, 1989.

10. Larrouturou, B. and Fezoui, L., "On the Equations of Multi-component Perfect or Real Gas Inviscid Flow," Lecture Notes in Math., 1402, 1988.

11. Larrouturou, B., "How to Preserve the Mass Fractions Positivity when Computing Compressible Multi-component Flows," J. Comput. Phys., 95, 59-84, 1991.

12. Chorin, A., "Random Choice Methods with Applications for Reacting Gas Flow," J. Comput. Phys., 25, 253-272, 1977.

13. Cohen, A. and Larsen, J., BRL Report 1386, 1967.

14. Maas, U. and Warnatz, J., "Ignition Processes in Hydrogen-Oxygen Mixtures," Comb. and Flame, 74, 53-69, 1988.

15. Kee, R. J., Miller, J. A., and Jefferson, T. H., "CHEMKIN: A General-Purpose, Problem-Independent, Transportable Fortran Chemical Kinetics Code Package," Rept. SAND 80-8003, Sandia National Laboratories, Livermore, CA, March 1986.

16. Stull, D. R. and Prophet, H., "JANAF Thermochemical Tables," National Standard Reference Data Series, U.S. National Bureau of Standards, 37, 1971.

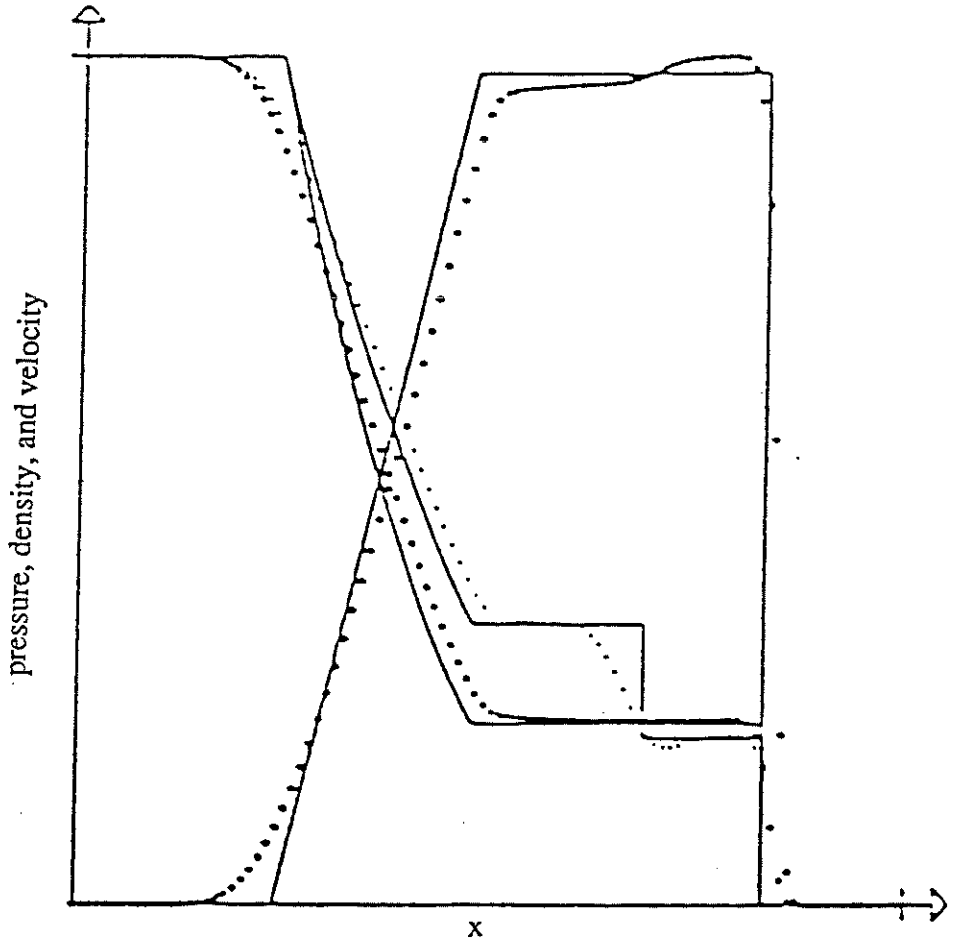

Figure 1 Mixing flow results by Larrouturou (1991) using Roe's scheme with first order accuracy

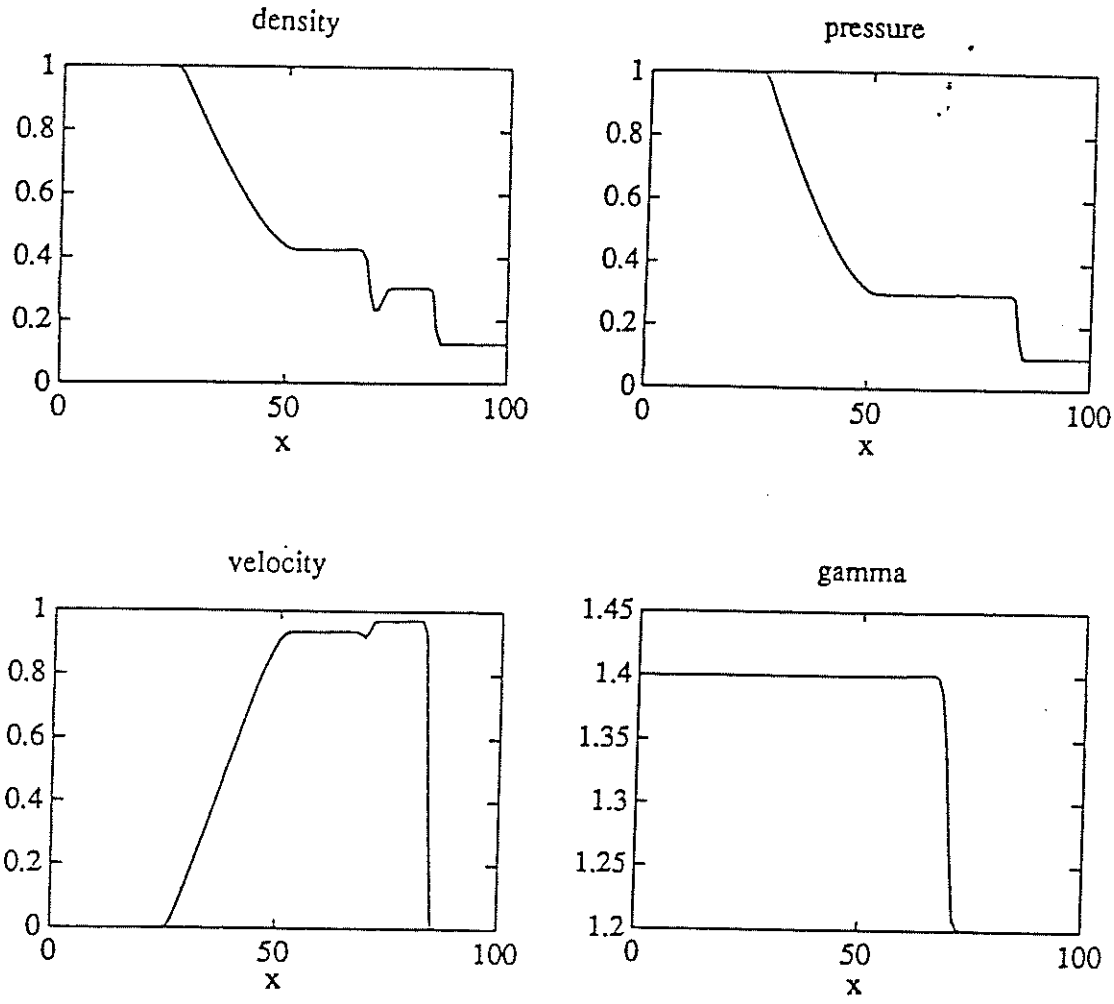

Figure 2 Mixing flow results by Karni (1991) using Roe's scheme with second order upwind differencing

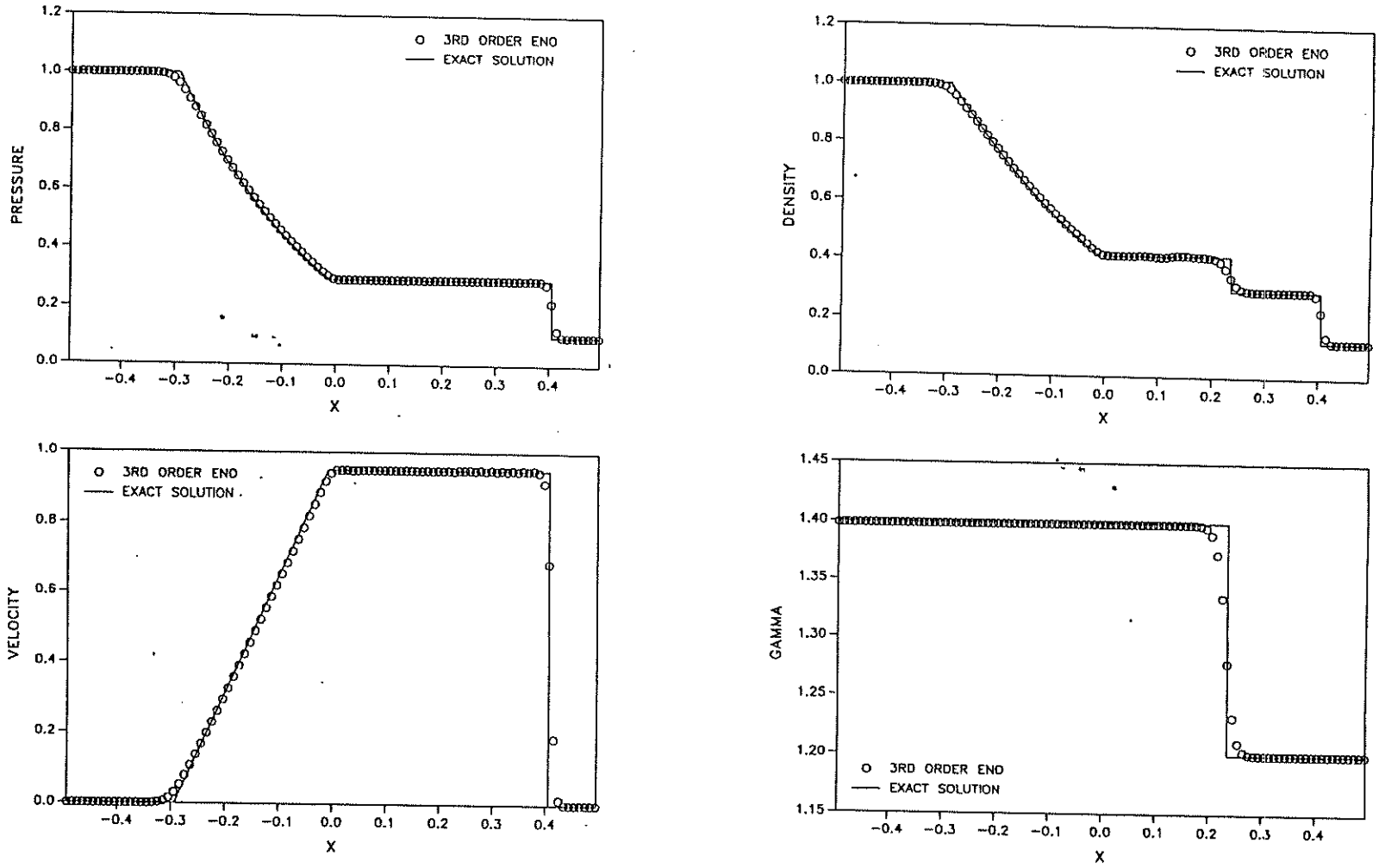

Figure 3 Third order accurate ENO scheme for mixing flow

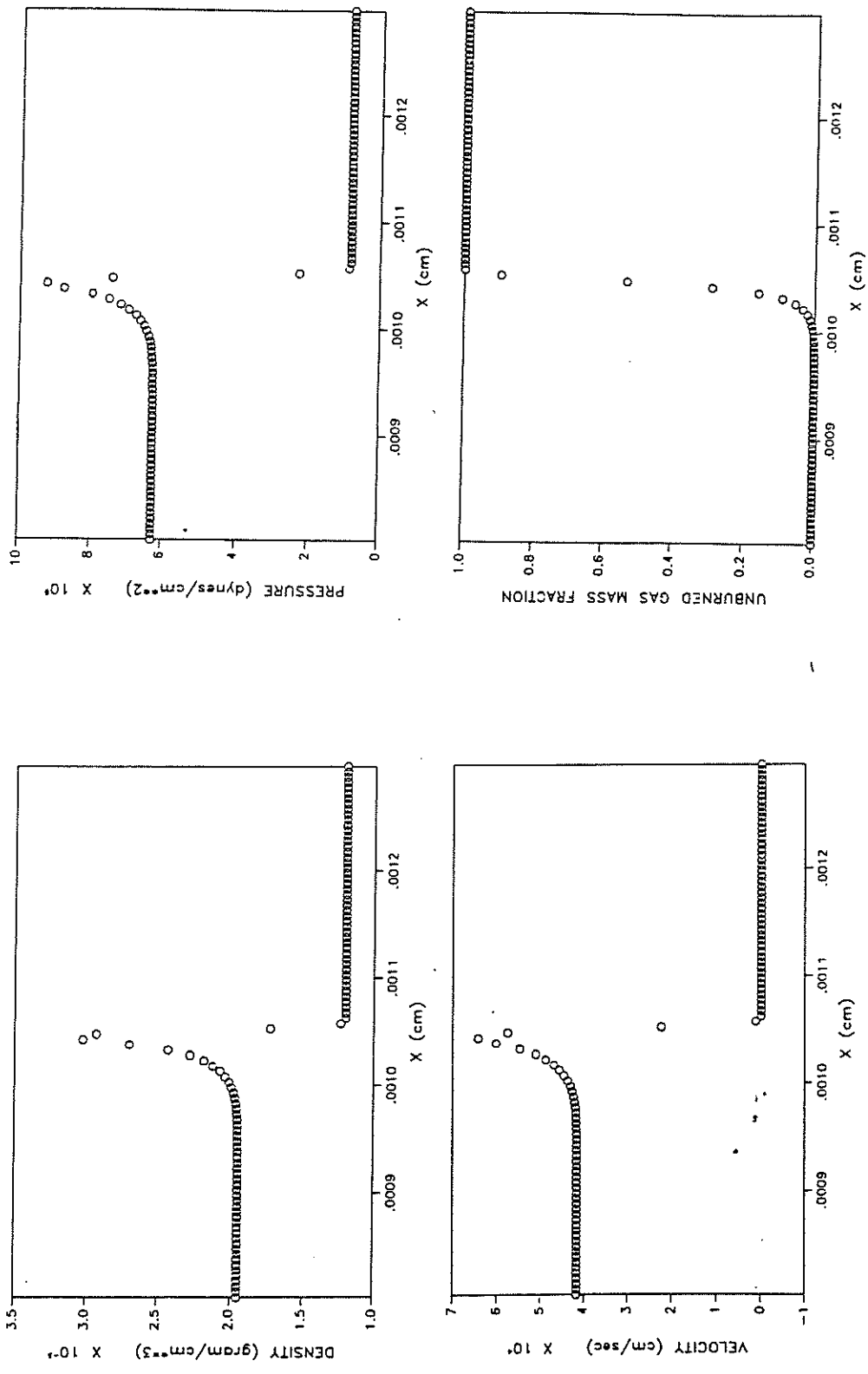

Figure 4 Chapman-Jouguet detonation wave, $\Delta x=5\times10^{-6}$ cm, $\Delta t=5\times10^{-12}$ s, at time $t=1\times10^{-8}$ s

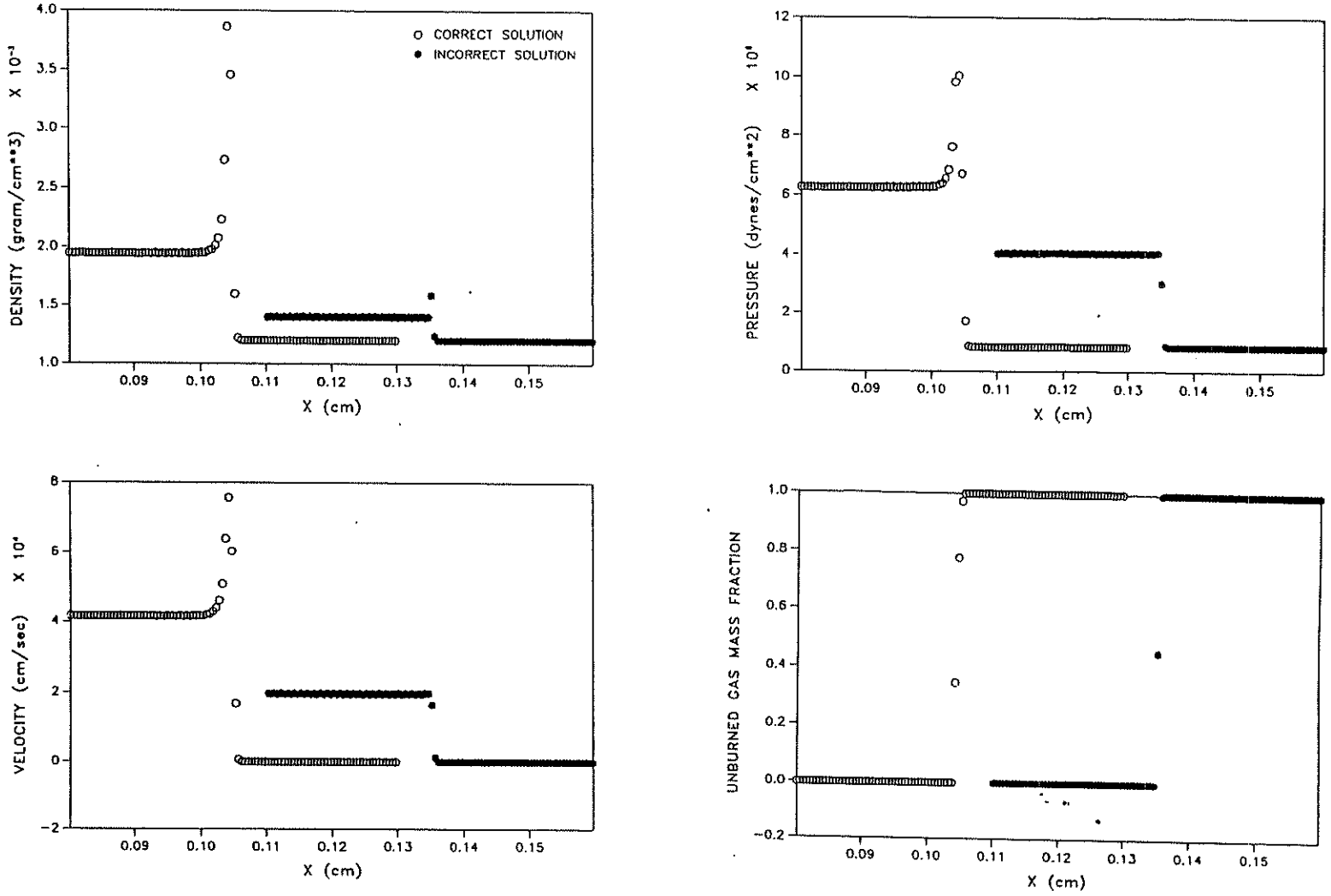

Figure 5 Chapman-Jouguet detonation wave, $\Delta x=5\times10^{-4}$ cm, $\Delta t=1\times10^{-10}$ s, at time $t=1\times10^{-6}$ s

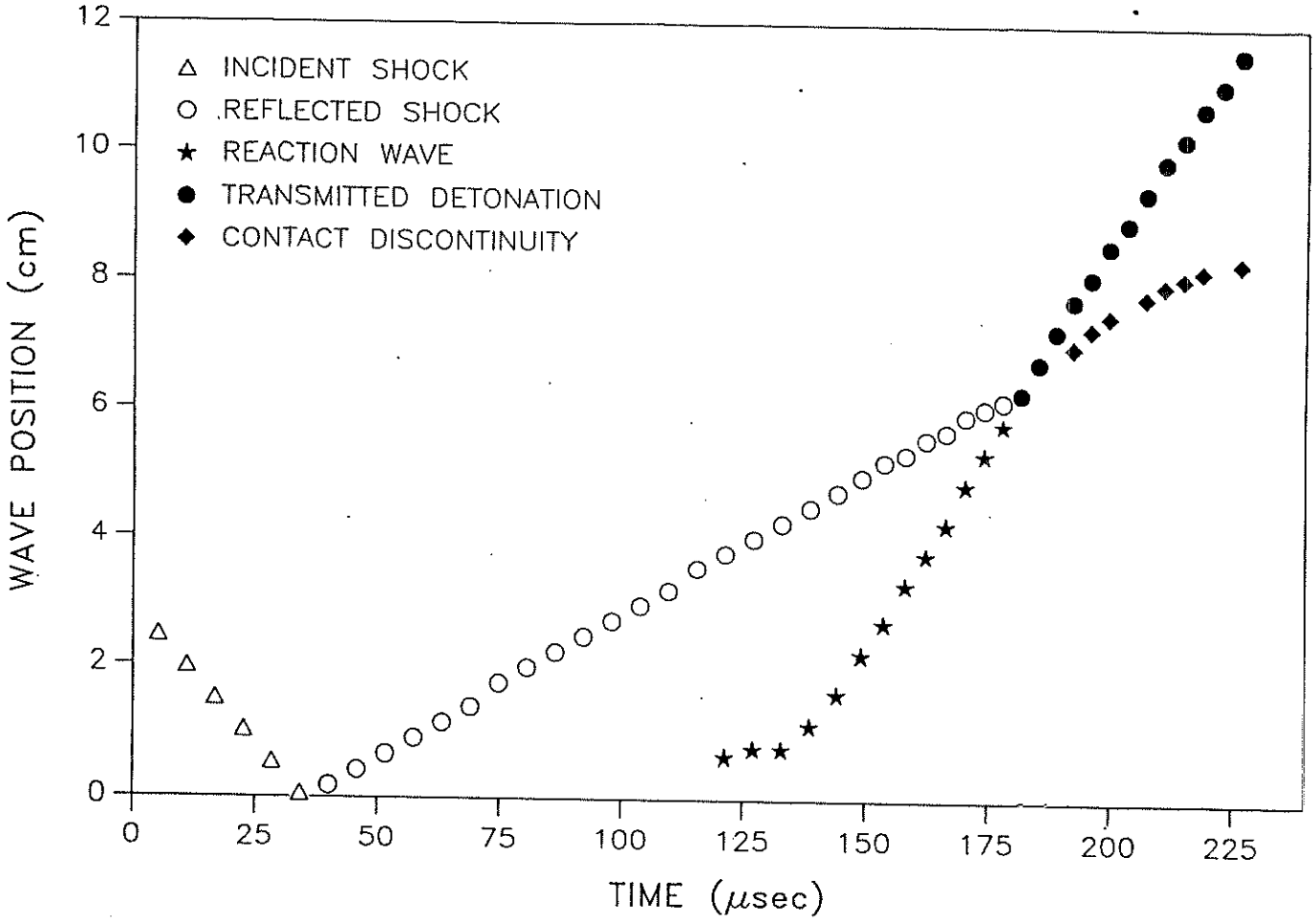

Figure 6 Calculated position of incident shock front, reflected shock front, reaction wave, transmitted detonation wave, and contact discontinuity for the ignition processes in hydrogen-oxygen-argon mixture

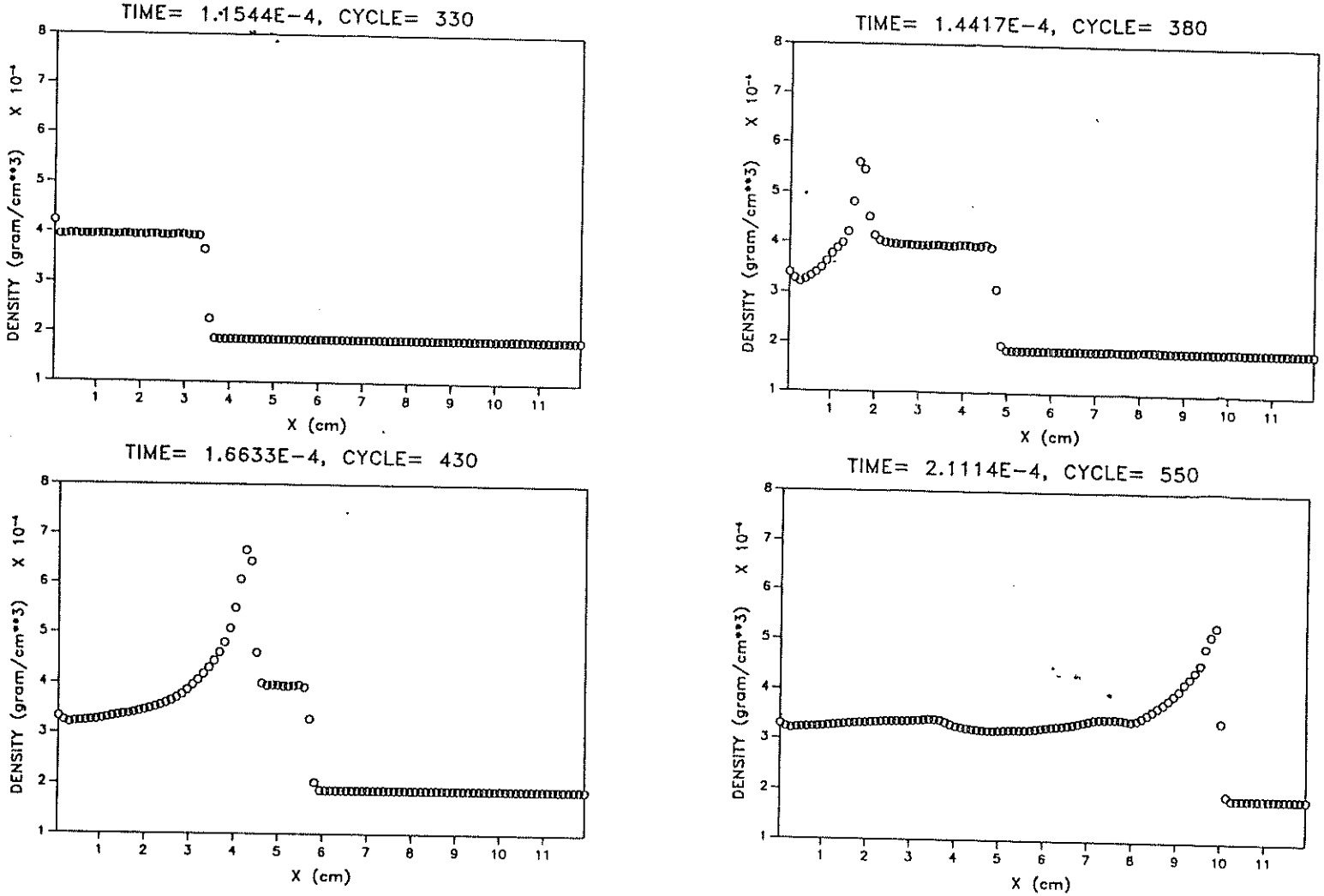

Figure 7 Density profiles for the ignition processes in hydrogen-oxygen-argon mixture at time t= 1.1544×10^{-4}, 1.4417×10^{-4}, 1.6633×10^{-4}, and 2.1114×10^{-4} seconds

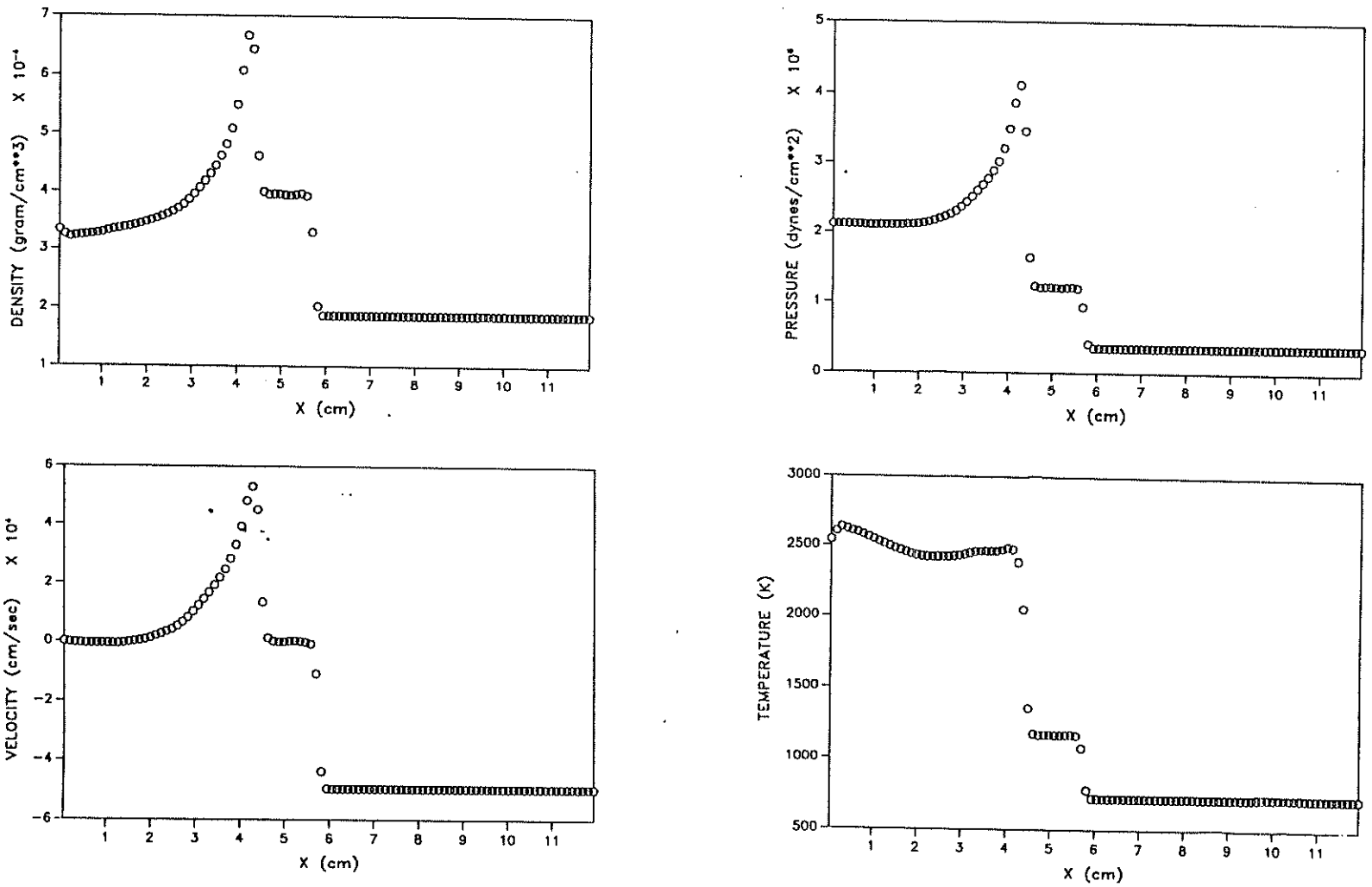

Figure 8 Density, pressure, velocity, and temperature profiles for ignition processes in hydrogen-oxygen-argon mixture at time t = 1.6633x10-4 sec.

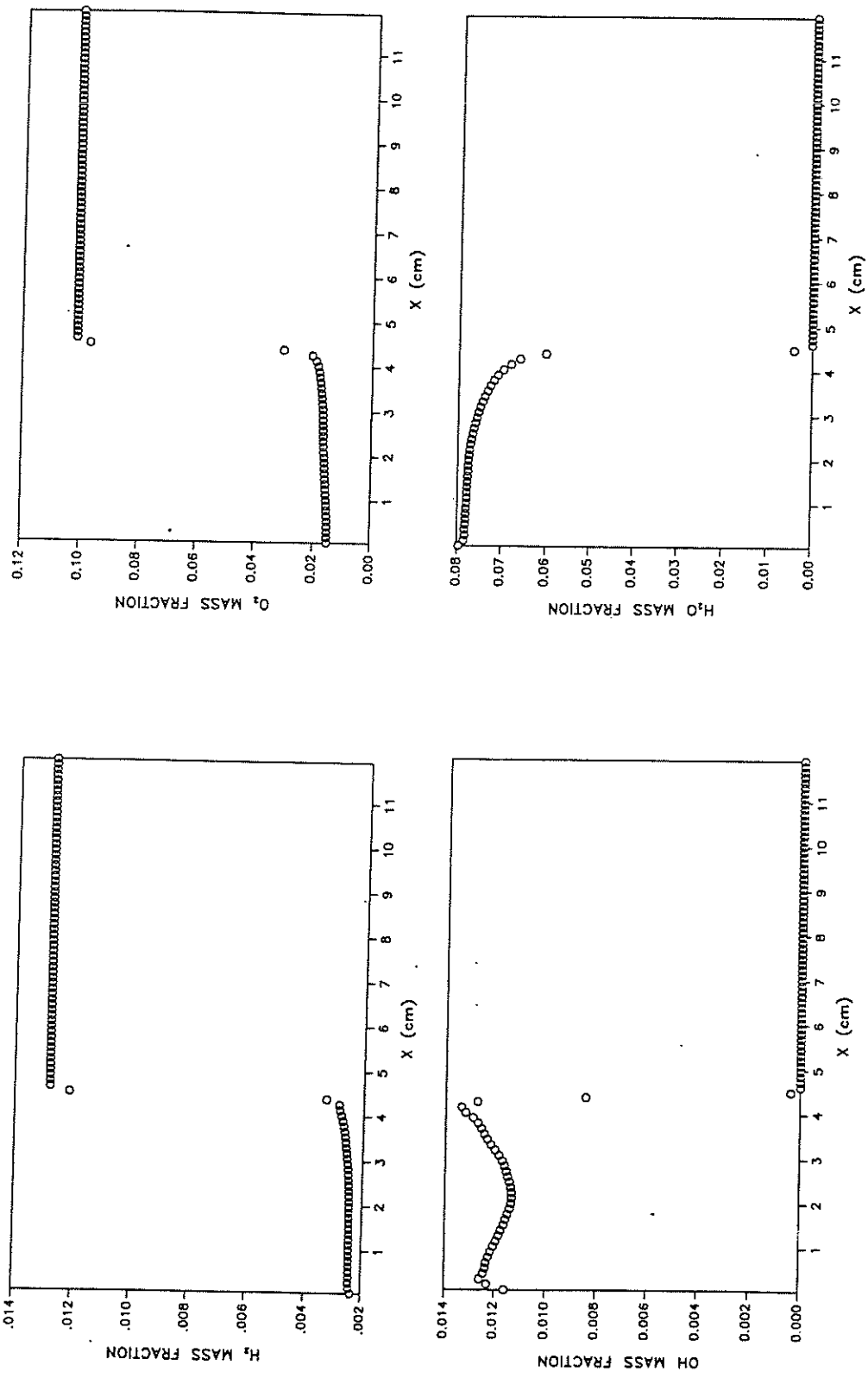

Figure 9 Species mass fraction profiles for the ignition processes in hydrogen-oxygen-argon mixture at time t = 1.6633x10-4 sec.

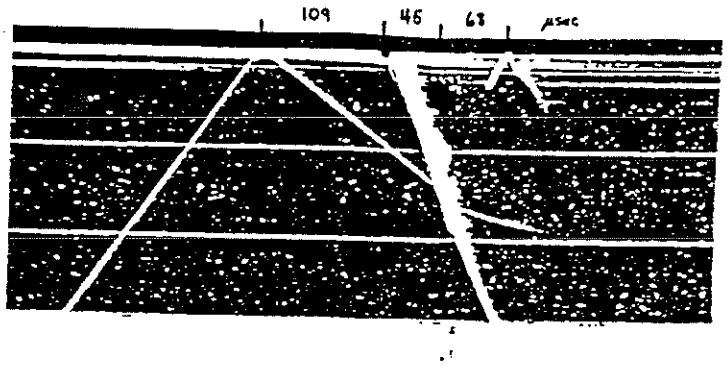

Figure 10a. Schlieren photograph with relative times marked for the ignition processes in hydrogen-oxygen-argon mixture by Cohen and Larsen (1967)

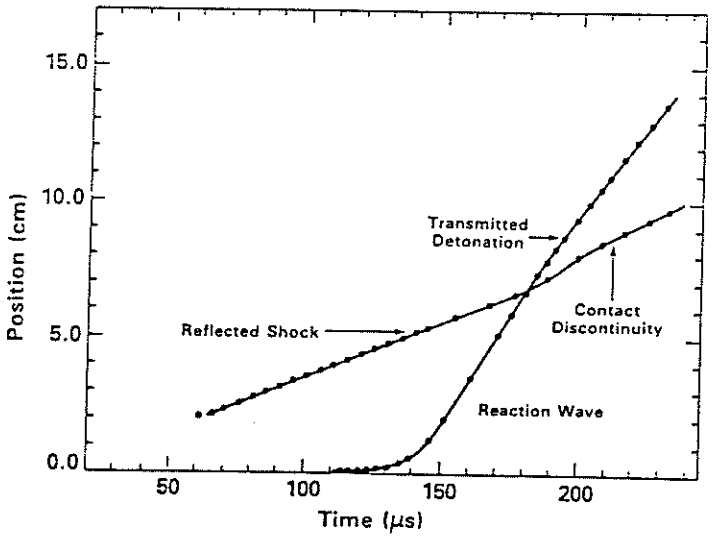

Figure 10b. Calculated results for the ignition processes in hydrogen-oxygen-argon mixture by Oran et al. (1982)